

Detection of cell surface calreticulin as a potential cancer biomarker using near-infrared emitting gold nanoclusters

This content has been downloaded from IOPscience. Please scroll down to see the full text.

2016 Nanotechnology 27 285101

(<http://iopscience.iop.org/0957-4484/27/28/285101>)

View [the table of contents for this issue](#), or go to the [journal homepage](#) for more

Download details:

IP Address: 128.40.219.50

This content was downloaded on 17/06/2016 at 08:27

Please note that [terms and conditions apply](#).

Detection of cell surface calreticulin as a potential cancer biomarker using near-infrared emitting gold nanoclusters

Bala Subramaniyam Ramesh, Emmanouil Giorgakis, Victor Lopez-Davila, Ashkan Kamali Dashtarzheneha and Marilena Loizidou

Research Department of Nanotechnology, Division of Surgery and Interventional Science, University College London, Pond Street, London NW3 2QG, UK

E-mail: b.ramesh@ucl.ac.uk

Received 27 February 2016, revised 9 May 2016

Accepted for publication 18 May 2016

Published 3 June 2016



CrossMark

Abstract

Calreticulin (CRT) is a cytoplasmic calcium-binding protein. The aim of this study was to investigate CRT presence in cancer with the use of fluorescent gold nanoclusters (AuNCs) and to explore AuNC synthesis using mercaptosuccinic acid (MSA) as a coating agent. MSA-coated AuNCs conferred well-dispersed, bio-stable, water-soluble nanoparticles with bioconjugation capacity and 800–850 nm fluorescence after broad-band excitation. Cell-viability assay revealed good AuNC tolerability. A native CRT amino-terminus corresponding peptide sequence was synthesised and used to generate rabbit site-specific antibodies. Target specificity was demonstrated with antibody blocking in colorectal and breast cancer cell models; human umbilical vein endothelial cells served as controls. We demonstrated a novel route of AuNC/MSA manufacture and CRT presence on colonic and breast cancerous cell surface. AuNCs served as fluorescent bio-probes specifically recognising surface-bound CRT. These results are promising in terms of AuNC application in cancer theranostics and CRT use as surface biomarker in human cancer.

Keywords: gold nanoclusters, quantum nanoparticles, calreticulin, theranostics, cancer biomarkers

(Some figures may appear in colour only in the online journal)

Abbreviations

AuNCs	Gold nanoclusters	MCF-7	Breast cancer cell lines
AuNC/MSA	Gold nanoclusters with mercaptosuccinic acid coating	MSA	Mercaptosuccinic acid
CRT	Calreticulin	NCs	Nanoclusters
ECL	Enhanced chemiluminescence	NIR	Near infrared
HT-29	Colorectal cancer cell lines	PBS	Phosphate buffer solution
HUVEC	Endothelial cell lines	TEM	Transmission electron microscopy
QDs	Quantum dots		

Background

Most tumours are only detectable when they attain a certain size; often, by the time of diagnosis they have already metastasised, thus impacting tumour resectability and outcome. This underlines the necessity for early cancer detection. To date,



Original content from this work may be used under the terms of the [Creative Commons Attribution 3.0 licence](https://creativecommons.org/licenses/by/3.0/). Any further distribution of this work must maintain attribution to the author(s) and the title of the work, journal citation and DOI.

standard diagnostic techniques such as cross-sectional imaging, tissue biopsy, biochemical investigations and immunoassays often lack sufficient specificity and sensitivity to detect malignancy at an early stage. An inspired approach to these shortcomings is the incorporation of colloidal semi-conductor-based fluorescent quantum nanoclusters (NCs). These nanoparticles may function as multimodal agents, allowing for rapid and highly sensitive biomarker detection and screening.

The use of ultra-sensitive fluorescence imaging techniques for biomolecular characterisation in the subcellular milieu has recently been a subject of interest [1]. These techniques rely on the efficiency of bio-unstable and sometimes highly toxic fluorescent labelling agents coupled to proteins, DNA or other biomolecules [2, 3]. These shortcomings have triggered research for discovery of more bio-stable fluorophores which could be deployable as probes for advanced *in vivo* theranostics, with particular focus on emission in the near infrared (NIR) range [4], to allow for maximum tissue penetration.

Noble metal-based, quantum-confined nanoclusters, composed of small number of Au or Ag atoms possess reasonably intense, size-dependent fluorescence [5]-and are significantly smaller than quantum dots (QDs). Furthermore, gold QD-based nanoparticles have been assessed as negligibly low in toxicity in biological systems at optimal concentration used [6]. There are several routes to the synthesis of gold nanoclusters (AuNCs) or QDs, including the widely used etching-based method, whereby small clusters are derived from large gold nanoparticles by thiols [7], biomolecules [8] or multivalent polymers [9]. Thiols have been popular both as stabilisers and coatings and a large number, such as tiopronin [10], phenylethylthiolate [11], thiolate α -cyclodextrin [12, 13], mercaptopropionic acid [14, 15], bidentate dihydrolipoic [16], dodecanthiol [17], and D-penicillamine [18–20] have been used to stabilise AuNCs. Although this technique allows for efficient production of AuNCs or QDs with multicolour fluorescence, it entails careful manipulations and long processing times.

Conjugation of NCs to antibodies against biomarkers provides targeting capabilities. One such candidate is calreticulin (CRT). CRT is a multifunctional, calcium-binding protein, predominantly residing in the endoplasmic reticulum. The protein normally acts as quality control chaperone by preventing misfolded proteins from proceeding to the Golgi apparatus [21]. CRT also acts as Ca^{2+} storage protein, thus playing a central role in the intracellular signal transduction systems and therefore in functions such as cellular proliferation and apoptosis¹. It also appears to act as a nuclear hormone receptor gene transcription modulator [22, 23].

CRT expression has been correlated with various cancers [24]. Due to its capacity of Ca^{2+} storage, CRT quite possibly becomes engaged to tumorigenic milestones such as migration, invasiveness and immortalisation [25]. It has recently been reported that CRT over-expression contributes to the

development and progression of pancreatic cancer [26], as well as gastric, oesophageal and ductal breast cancer, where it has been positively correlated with poorer prognosis [27, 28]. Perhaps to make things more perplexed, it has been supported that it plays a pivotal role in malignant cells' engulfment [29] and facilitates increased cancer immunogenicity [30]. Conventional anticancer drugs, such as anthracyclines, induce CRT translocation to the cell surface. This translocation potentially acts as an immune system leverage during chemotherapy [31]. Finally, it was recently reported that CRT is the dominant pro-phagocytic signal on multiple human cancers, such as acute myeloid leukaemia, non-Hodgkin's lymphoma, bladder, ovarian cancer and glioblastomas, and its action is counterbalanced by CD47 [32]. The above multifaceted attributes make CRT a potential biomarker with promising diagnosing, tumour grading and therapeutic potential.

In this study we embarked on the development of a simple one-pot synthesis of ultra-small photo-luminescent AuNCs with NIR emission in an aqueous solution. This was achieved with slow reduction using specified amount of DMF and stabilising with the thiol derivative mercaptosuccinic acid (MSA) as a functional coating to facilitate conjugation to biomolecules. For the purpose of targeting and localisation for bio-imaging studies, an anti-CRT antibody was raised and conjugated within the desirable physiological pH range obtained with MSA. We also aimed to investigate the detectability of CRT on the surface of cancer cells and to further explore cancer cells' targeting with fluorescent anti-CRT AuNCs.

Methods

Reagents

All chemicals were of analytical grade. MSA, gold (III) chloride trihydrate ($\text{HAuCl}_4 \cdot 3\text{H}_2\text{O}$), Dimethylformamide (DMF) and N-(3-dimethylaminopropyl)-N-ethylcarbodiimide hydrochloride (EDC) were purchased from Sigma-Aldrich (UK). In all preparations high purity deionised water from a Millipore system was used.

Production and purification of anti-calreticulin peptide IgG antibodies

To generate anti-sera to human CRT protein, a synthetic peptide of 15 amino acid (NH_2 -Met-Leu-Leu-Ser-Val-Pro-Leu-Leu-Gly-Leu-Ala-Val-Ala-Pro-Ala- NH_2) corresponding to the amino terminus of this protein was chemically synthesised using the Fmoc solid phase strategy. The peptide was conjugated to keyhole limpet haemocyanin (KLH) using glutaldehyde. The KLH conjugated peptide was injected into New Zealand white rabbits (1 mg/rabbit) (Intra muscular, IM) for polyclonal antibody production. The IgG components were isolated from the rabbit serum using 50% saturated ammonium sulphate solution and concentrated using 100 KDa cut off centricon centrifuge tubes. Antibody specificity to the peptide

¹ Second messenger systems at the US national library of medicine medical subject headings (mesh).

antigen was established by routine enzyme-linked immunosorbent assay and western blots of cell homogenates (data not shown). The resultant anti-CRT was used for QD conjugation experiments and for all subsequent *in vitro* localisation and detection studies.

Synthesis of MSA-stabilised gold nanoclusters (AuNC/MSA)

The method used in this study involved a modification of earlier methods to obtain visible fluorescent gold QDs [33]. All glassware used in this preparation were cleaned in freshly prepared aqua regia (HCl: HNO₃, 3: 1 v/v) and rinsed stringently (x3) in water prior to preparation. Instead of using neat organic solvent, purified de-ionised water (pH 6.5) was used as the major solvent. The precursor solution was prepared with a mixture of MSA (50 mM) and HAuCl₄ (25 mM) in 50 ml of water. After vigorous stirring of the precursor mixture for 5 min, using a homogenizer at maximum speed, 500 μ l (12.9 M) of the polar aprotic solvent, DMF (73.09 g mol⁻¹), was added to the mixing precursor solution for another 5 min at room temperature. This mixture was then processed by hydrothermal treatment (autoclave) at 121 °C for 25 min to produce quantum confined MSA–AuNCs with NIR emission at \geq 800 nm on cooling to room temperature.

This method is novel in that others have used neat DMF with long heating times with multiple steps to produce nanoclusters not necessarily emitting in the infra-red region.

AuNC characterisation

The fluorescence spectra of AuNCs, either native or with chemical modifications, were mapped to check that the NC fluorescence was not quenched; in order to use them for different biomedical applications, spectra were taken by a spectrofluorometer (Ocean Optics, USB 2000+) with an excitation source at 375 or 630 nm. The quantum yield (QY) at 375 nm excitation of MSA–AuNCs in aqueous solution at room temperature was determined using the comparative method which relies on the use of fluorescence standards with known QY of rhodamine 6G (0.95 in ethanol) [34]. The QY of MSA–AuNCs was estimated to be 0.6 using rhodamine 6G as a standard.

Transmission electron microscopy (TEM) (Phillips CM 120) was used for visualisation and to obtain the size of AuNCs. To determine the size and shape of the MSA-coated NCs, a set of 1:100 serial dilutions were made of MSA-coated NC with PBS and the optimum dilution was chosen. A drop of the samples was mounted on to a Piloform (TAAB) coated G300HS copper electron microscopy grid (Gilder) and allowed to air dry. The grids were examined with a CM120 (Philips) TEM at 3.0×10^5 magnification.

Cell culture

All cell cultures were routinely maintained in standard growth conditions (37 °C, 5% CO₂). The cancer cell lines MCF-7 (breast adenocarcinoma, ECACC, Sigma Aldrich) and HT29 (colorectal adenocarcinoma, ECACC) were maintained in D-MEM containing 1 mM pyruvate, 2 mM glutamine and

10 mM HEPES, supplemented with 10% foetal bovine serum (FBS) and 100 IU penicillin and 100 μ g ml⁻¹ streptomycin, human umbilical vein endothelial cells (HUVECS) were maintained in PromoCell endothelial cell growth medium with supplement mix (PromoCell GmbH) 5% FBS supplemented with growth factors. Cells were routinely passaged (trypsin) and for further stocks or plated into multiwell plates (Corning USA) for the investigations below.

Cell viability assay

The viability of cells treated with AuNCs and appropriate controls was measured with the alamar blue (AB) metabolic assay. Cells (1×10^4 /well) were plated into 96 well plates and after 48 h growth the medium was removed and replaced with different concentrations of coated and precursor AuNCs or constituent compounds. The selected concentrations of coated and precursor AuNC were as following; 0, 50, 100, 150, 200 μ g ml⁻¹ were added in replicates of 12 wells in a 96-well plate. The incubated cells were monitored over the time course of 48 h.

After 24 h incubation, 20 μ l of AB solution (10 X) were added to medium in each well and incubated for another 4 h. The viability indicator, which uses the natural reducing power of living cells to convert resazurin to the absorbing molecule resorufin, was adopted to assess toxicity. The amount of absorbance was proportional to the number of metabolically active viable cells. Absorbance read as optical density was measured (excitation 530; emission 620) with 600 nm as a reference wavelength, using a 96-well plate reader (Helena Biosciences, Sunderland, UK) in a Multiscan MS UV–visible spectrophotometer (Labsystems, Ashford, UK).

Preparation of anti-calreticulin conjugation to AuNC/MSA (anti-CRT–AuNCs)

Fluorescent AuNC/MSA solution was diluted with equal volume of cold ethanol and centrifuged at 10 000 g for approximately 30 min. The precipitated AuNC/MSA was vacuum dried to be obtained as a powder. The precipitated dried AuNC/MSA (approximately 1 mg) was re-suspended in 1 ml phosphate buffer saline. The obtained coated AuNC/MSA (1 ml) solution was conjugated to the anti-CRT using EDC as an acylating agent. Briefly, 200 μ l of AuNC/MSA solution (1 mg ml⁻¹) was mixed with 200 μ l EDC (1 mg ml⁻¹) in PBS for 30 min at room temperature. 100 μ l of anti-CRT solution (5 mg ml⁻¹) was added to the activated mixture and agitated gently for 2 h at room temperature.

To separate the reagent and unconjugated AuNC/MSA, membrane centrifugal columns (centricon) with a cut off of 100 kDa were centrifuged at 5000 g with UV monitoring at 280 nm of the retained samples. Immuno-chemiluminescence detection was carried to further validate conjugation of the AuNC-anti-CRT via dot blot [35]. There were no changes in fluorescence intensity or shift in spectra position despite modification.

To determine the number of antibodies per nanocluster, calculation was carried out based on the method applied to

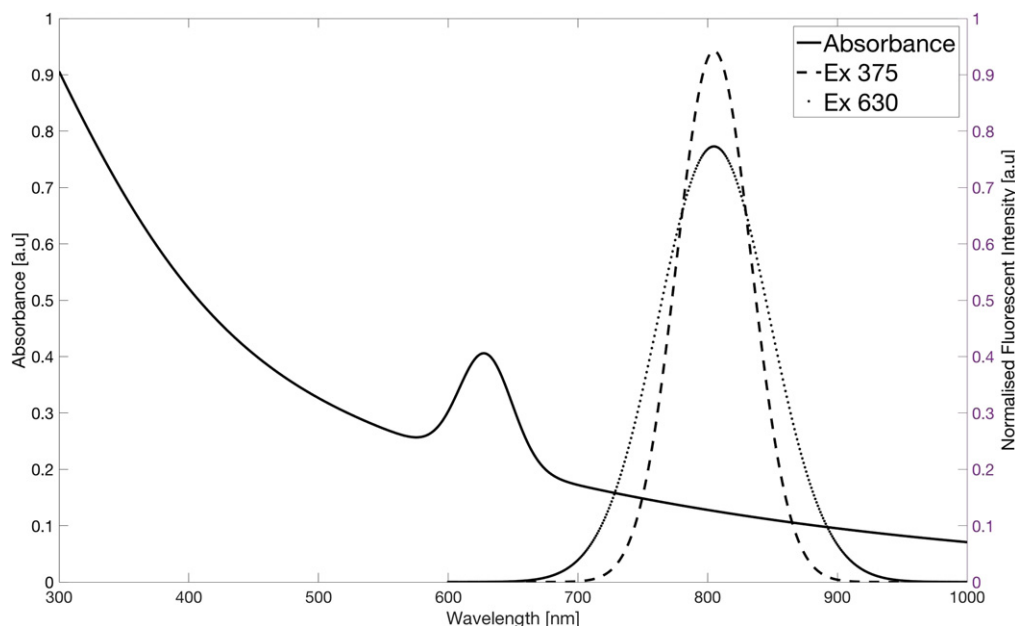


Figure 1. Absorption and emission profiles of MSA–AuNCs. The MSA–AuNCs are characterised by broad absorption spectrum (solid line) and emission profiles at 800 nm, excited at 375 nm (dashed line) and 630 nm (dotted line).

equivalent bioconjugated QDs. Accordingly we obtained ~ 0.5 IgG molecules per AuNC for a 1:2 IgG/AuNC molar ratio. The purified bio-conjugated nanoclusters defined as anti-CRT–AuNCs conjugated to anti-CRT were collected and stored at $+4^\circ\text{C}$ until further use.

Cell incubation with anti-CRT–AuNC and anti-CRT

Two different cancer cell lines were used; HT-29 (colon) and MCF-7 (breast). Endothelial primary cells (HUVECs) were used as non-malignant cell controls. To study the targeting and imaging of the conjugated anti-CRT–AuNC, cells were grown routinely in 24 well plates. After 36 h of incubation (70% confluence), the cells were rinsed with sterile PBS and 1 ml of the corresponding fresh media with 5% FB with anti-CRT–AuNC at 1:500 titre to the plates. Cells incubated with unconjugated AuNCs were also incubated with the cells and served as controls. Anti-CRT antibodies were also pre-incubated with cells to validate the specificity by blocking the presence of any CRT on the cell surface. All cells were incubated for 1 h at 37°C in a humidified 5% CO_2 atmosphere. After 1 h the cells were washed with PBS (pH 7.4) and fixed with 4% paraformaldehyde for 30 min at room temperature. After washing three times with PBS the plates were directly imaged under confocal laser scanning microscope.

Cell imaging with confocal microscopy

Images were acquired by fluorescent microscopy (Nikon Eclipse TE 300). The PCM scanning head was mounted on an inverted optical microscope (Nikon Eclipse TE 300), which can operate in fluorescence, reflection and phase contrast modes, and it was provided with Plan Fluor dry objective ($20\times/\text{NA} = 0.5$). He–Ne laser (488 nm) and 543 nm are the

sources, housed in a common module, providing the excitation beams that are delivered to the scanning head through a single-mode optical fibre. Photomultiplier (PMT) tubes are placed within the control unit, and the collected light transported via high-transmission optical fibres. This greatly minimises the electronic noise at the PMT output. Images were collected with excitation at 488 nm laser, with 630 nm LP (long pass) emission filter for the NIR emitting antiCRT–AuNC positive samples (red pseudocolour).

Results

Synthesis of AuNCs

Fluorescent AuNCs were prepared in one pot technique by reducing gold salt with minimum amount of DMF in the presence of MSA introducing sequentially, starting with MSA and then DMF in aqueous solution with vigorous mixing. A light brown colour of the solution suggests formation of ultra-small non-fluorescent NCs. Subjecting the mixture to hydrothermal heating at 121°C for 25 min and cooling produced NIR-emitting NCs. Of significant importance is the non-appearance of fluorescence prior to the heating suggesting that luminescence originates from high temperature slow reduction by DMF of the AuNCs capped with MSA.

A prominent fluorescent emission peak was observed at 800 nm in the NIR region in aqueous solution upon excitation at 375 and 630 nm (figure 1). TEM of MSA–AuNCs indicated an average core diameter of 2 nm (figure 2), the hydrodynamic diameter assessed by dynamic light scattering was 3.5 nm. The ultra-small nanoparticle size in aqueous solution well below 5 nm imparts AuNCs as suitable fluorescence probes for bio-conjugating and high resolution

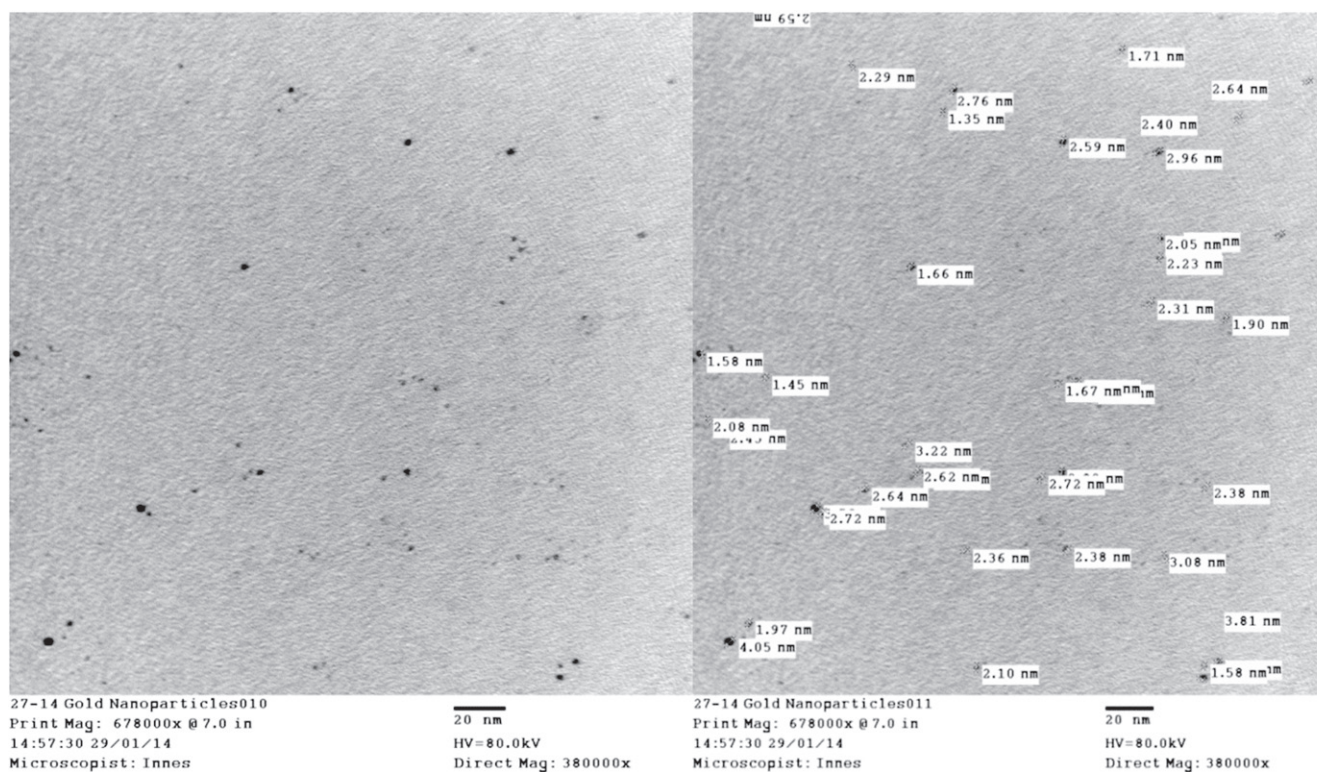


Figure 2. TEM image of dispersed AuNCs showing average diameter.

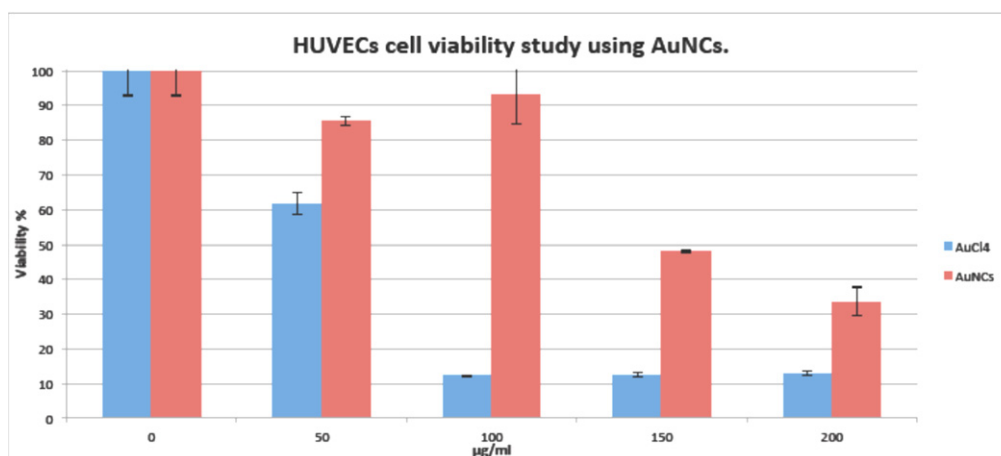


Figure 3. The effect of AuNCs and HAuCl₄ (free precursor salt) on cell viability of human umbilical vein endothelial cells (HUVECs). Cells were treated with various concentrations of NCs and free salt for 24 h. Cell viability taken as equivalent to metabolic activity was measured by alamar blue absorbance assay (\pm SD; $n = 4$; $p < 0.05$ compared with control).

imaging [36]. Further observation over 1 year of storage in sterile buffer solution demonstrated no precipitations or optical deterioration. These properties are appealing if compared to other non-metal fluorophores and make these nanoparticles compatible for biological applications.

Toxicity of AuNCs and their precursor salts in cancer and non-cancer cells

To examine possible toxic effects, cancerous and non-cancerous cells were treated with MSA-coated AuNCs and

the precursor free salt (HAuCl₄) for 24 h (figures 3–5). As shown graphically, AuNCs dose-dependently decreased the cell viability, illustrated as a gradual decline in metabolic conversion in the presence of 0–200 $\mu\text{g ml}^{-1}$ AuNCs. Significant cell death in the case of HUVECs was observed with MSA-coated AuNCs at concentrations of 50 $\mu\text{g ml}^{-1}$ and above. Cancer cells seem to be robust and managed to cope at higher doses than HUVECs. However, with precursor salts there was a dramatic steep decline in viability, especially in the non-cancerous HUVECs (figure 3) as compared to the cancerous cells (HT29, MCF7; figures 4 and 5). Generally, cell

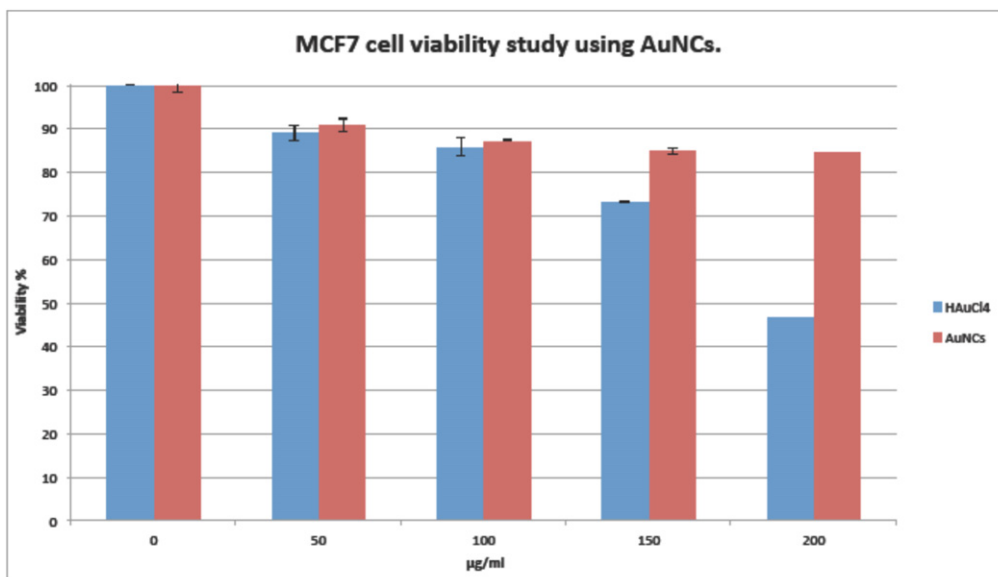


Figure 4. The effect of AuNCs and HAuCl₄ (free precursor salt) on cell viability of MCF-7 breast cancer cells treated with various concentrations of NCs and free salt for 24 h. Cell viability taken as equivalent to metabolic activity was measured by alamar blue absorbance assay (\pm SD; $n = 4$; $p < 0.05$ compared with control).

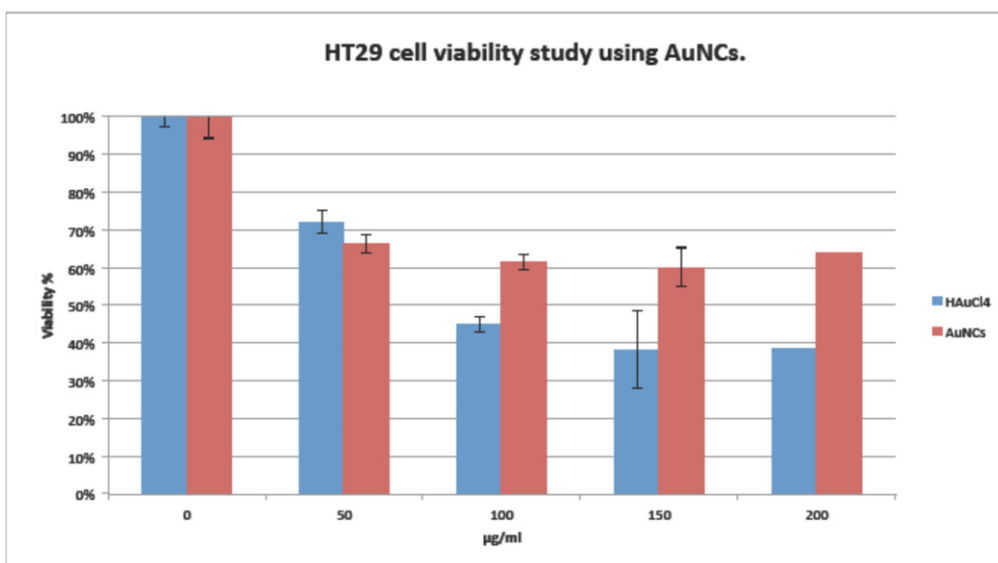


Figure 5. The effect of AuNCs and HAuCl₄ (free precursor salt) on cell viability of HT-29 colorectal cancer cells treated with various concentrations of NCs and free salt for 24 h. Cell viability taken as equivalent to metabolic activity was measured by alamar blue absorbance assay (\pm SD; $n = 4$; $p < 0.05$ compared with control).

viability levels at the maximum salt doses used were $<20\%$ for HUVECs but $>50\%$ for cancer cells.

Fluorescence imaging of anti-CRT–AuNCs in cancer and non-cancer cells

Utilisation of AuNCs as an efficient targeted contrast agent for *in vitro* or *in vivo* imaging necessitates further modification by conjugating with specific bio-recognition molecules. We selected antibodies targeted to a short peptide corresponding to the amino terminus of human CRT. This protein

has been primarily located on most cancer cells and is a suitable bio-conjugate to AuNCs. Water-soluble AuNCs were conjugated to anti-CRT using water-soluble EDC method [37, 38]. The anti-CRT–AuNC conjugates were delivered to live cells by incubating for 1 h and fixed with 4% paraformaldehyde in PBS. Figure 6 shows confocal images of cells with strong fluorescence localised to the surface of HT29 and MCF7 cancer cells incubated with anti-CRT AuNCs, compared to cells incubated with untargeted AuNCs (figures 6(A) versus (B); (D) versus (E)). In order to further validate CRT localisation on the extracellular membrane of cells, incubation

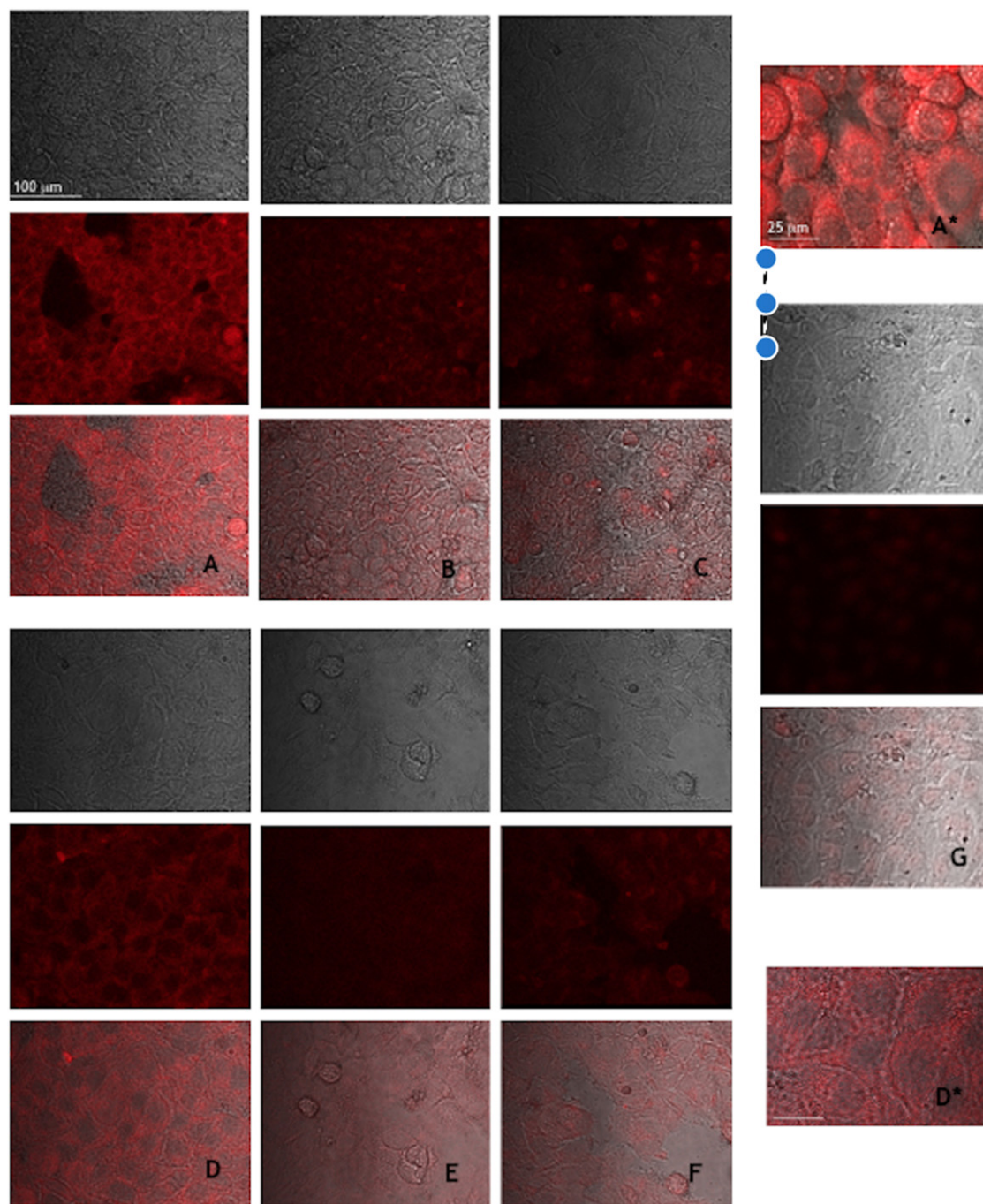


Figure 6. Confocal microscopic analysis of cells incubated with AuNCs. Cells were grown in 24-well plates and incubated for 1 h with unconjugated AuNCs or anti-CRT–AuNC (conjugated to anti-CRT antibody), with or without pre-incubation with anti-CRT Ab to demonstrate competitive inhibition. (A) Anti-CRT–AuNC binding to HT-29 colorectal cancer cells. (B) Unconjugated AuNC binding to HT-29 cells. (C), (B) anti-CRT–AuNC binding to HT-29 colorectal cancer cells which were pre-incubated by anti-CRT Ab. (D) Anti-CRT–AuNC binding to MCF-7 breast cancer cells. (E) Unconjugated AuNC binding to MCF-7 cells. (F) Anti-CRT–AuNC binding to MCF-7 breast cancer cells which were pre-incubated with anti-CRT Ab. (G) Anti-CRT–AuNC binding to HUVECs (serving as non-cancer control cells). For the triple-image groups (A)–(G): top channels show the transmission images, middle channels show fluorescence and bottom channels are the merged images of the two. (A*) (HT29 colorectal cancer) and (D*) (MCF7 breast cancer) are magnifications or the equivalent merged images. NIR emitting AuNCs were imaged using 488 nm laser excitation with 630 nm LP emission filter (red pseudocolour).

was also performed on control non-cancer cells, HUVECs, which showed minimal/no fluorescence (figure 6(G)). To further validate specificity, antibody blocking was carried out on cancerous cells. HT29 and MCF7 cancer cells which were

pre-incubated with anti-CRT antibody (prior to exposure to targeted AUNCs) showed considerably less fluorescent signal indicating competitive inhibition of anti-CRT AuNC binding (figures 6(A) versus (C); (D) versus (F)).

Discussion

In this study we embarked on the development of a simple one-pot synthesis of ultra-small photoluminescent AuNCs with NIR emission in an aqueous solution, with the view to use them for biomarker targeting; and chose CRT as the exemplar target molecule.

NIR emitting AuNCs (800 nm) can be prepared in a one step by reducing gold salt with DMF in the presence of MSA in aqueous environment. Control mixtures without MSA or DMF resulted in no observable emission, indicating that quantum confinement can only be obtained in the presence of DMF and MSA on hydrothermal processing. DMF was one of the standard organic compounds used as a solvent for various processes, including the preparation of colloids [39] containing metals in their composition. We demonstrated the ability of DMF to reduce Au⁺ ions at high temperature in the presence of MSA, with formation of dispersions of AuNCs being assembled in a short time. Our goal was to modify the gold salts with MSA. The latter was selected as a capping ligand as, from its molecular structure (pKCOOH = 3.30 and 4.94), it was expected to possess combined properties of both mercaptopropionic acid (MPA, pKCOOH = 4.32) and thioglycolic acid (TGA, pKCOOH = 3.53). It is known that MPA and TGA can only stabilise efficiently semiconductor based nanocrystals in alkaline aqueous solution [40], whereas MSA can stabilise in weak acidic solution within the desirable physiological pH range. As a normal thiol derivative, chemical adsorption to the nanoparticle surface through Au–S bonding is anticipated. Similar to MPA and TGA, MSA has dissociable carboxylic groups which enable its electrostatic interaction to maintain stability. Finally, since it is soluble, further surface modifications can be facilitated in aqueous phase without the risk of irreversible precipitation by biological ligands. Our resultant MSA-coated NCs were within the expected nano-range size. Interestingly, the MSA-AuNCs exhibit a distinct absorption peak at 620 nm, which may arise from electronic transition between the shell and the gold cluster core.

Nano-materials with fluorescent emission on excitation have been developed by many groups for biological labelling and imaging. However, compared with visible fluorescence emitting nano-materials, those with NIR emission (650–900 nm) have superior advantages in biological imaging due to relatively maximum transparency and minimum auto-fluorescence in living tissues [41, 42]. To date various kinds of semi-conductor based NIR emitting nanomaterials, such as QDs, have been synthesised such as mercury sulphide (HgS), cadmium/mercury/tellurium (CdHgTe), cadmium phosphide (Cd3P2) and cadmium/lead/sulphide (CdPbS) [43, 44], with unresolved concerns about potential toxicity. Very recently, the manufacture of NIR-emitting nano-material hybrids containing gold and silver NCs have been reported for biological applications [45, 46].

To examine toxicity, colorectal HT29 and breast MCF7 cancer cells and HUVECs were treated with MSA-coated AuNCs and its precursor free salt for 24 h; HUVECs were used as a non-cancerous cell control. Generally, AuNCs were only toxic at high concentrations, compared to the free salt precursors;

and cancer cells were much more resilient than endothelial cells. In the latter case, the tolerance of cancer cells may be due to altered redox functionalities. Furthermore, the possibility of intracellular reactive oxygen species levels' elevation and subsequent mitochondrial dysfunction by the gold salts might be at play here. This necessitates further verification in future studies. Besides maintaining cellular metabolism, mitochondria have also been shown in studies to perform important functions in the signal transduction for apoptosis. HUVECs being of vascular origin, very little is known of nanoparticles or QDs effect on endothelial function when they penetrate vasculature through injection as delivery or imaging agents. Generally, recent reports of AuNCs tested *in vitro*, for example in dendritic cells, have not reported noticeable toxicity levels [46].

Having manufactured AuNCs, our second aim was to use them to target CRT to determine its usefulness as a cancer biomarker. This molecule is a multifunctional, calcium-binding protein, usually found the endoplasmic reticulum, which aids correct protein folding. We aimed to demonstrate the presence of CRT predominantly on the membrane surface of cancer cells. We further aspired to demonstrate on *in vitro* confocal microscopy that cancer cells can be targeted with fluorescent anti-CRT gold NCs; and to develop in the future concomitant photothermal effect in the presence of iron oxide magnetic nanoparticles as a potential therapy.

Although induced CRT translocation to the cancer cell surface has already been demonstrated, we discovered that CRT is expressed on the surface of tumour-derived cells of the solid cancers investigated, in the absence of any form of induction. In normal cells, CRT functions as a calcium-binding protein, predominantly present in the endoplasmic reticulum, where it acts as a chaperone, promoting protein folding. The results from our present study indicate that CRT is present on the membrane surface of cancerous cells; its novel labelling on cancerous cell surface by anti-CRT conjugated AuNCs suggests that CRT translocates to the cell surface during carcinogenesis, perhaps inducing immunotolerance of the malignant cells among other functions. There have been previous studies linking its association to various cancers [47]. The mechanistic pathways involving CRT and its role in cancer remain largely unknown, although there have been studies about its role in immunogenic cell death. Elucidation of the mechanisms by which cell-surface CRT may facilitate cancerous cells' evasion from immune cell death, may allow its potential application as a theranostic biomarker in the personalised treatment of various cancers with CRT cell surface expression.

In conclusion, we have developed a simple synthesis route for the production of high quality metal-based NCs using NIR-emitting AuNCs as a probe and MSA as a coating and stabiliser. Compared to most semiconductor-based fluorophores, our approach to the synthesis of biostable, aqueous noble metal NCs emitting in the NIR is simple, economical, reproducible and environmentally friendly. The AuNCs produced were further deployed to demonstrate the universal presence of CRT on the cell surface of various human solid cancer cell lines.

The above findings blaze the path for the application of NIR-emitting AuNCs as theranostic nanobioprobes in human cancer and the use of CRT as a cancer biomarker; further knowledge and exploitation of AuNCs quantum properties, jointly with the yet to be fully elucidated CRT role as a modulating factor in immune-mediated cancerous cell death may facilitate the use of AuNC targeting of CRT in the personalised treatment of CRT cell surface-positive human cancer, among others.

References

- [1] Joo C, Balci H, Ishitsuka Y, Buranachai C and Ha T 2008 Advances in single-molecule fluorescence methods for molecular biology *Annu. Rev. Biochem.* **77** 51–76
- [2] Resch-Genger U, Grabolle M, Cavaliere-Jaricot S, Nitschke R and Nann T 2008 Quantum dots versus organic dyes as fluorescent labels *Nat. Methods* **5** 763–75
- [3] Nienhaus G U 2009 Single-molecule fluorescence studies of protein folding *Methods Mol. Biol.* **490** 311–37
- [4] Cheng Z, Wu Y, Xiong Z, Gambhir S S and Chen X 2005 Near-infrared fluorescent RGD peptides for optical imaging of integrin α v β 3 expression in living mice *Bioconjug. Chem.* **16** 1433–41
- [5] Xie J, Zheng Y and Ying J Y 2009 Protein-directed synthesis of highly fluorescent gold nanoclusters *J. Am. Chem. Soc.* **131** 888–9
- [6] Retnakumari A, Setua S, Menon D, Ravindran P, Muhammed H, Pradeep T, Nair S and Koyakutty M 2010 Molecular-receptor-specific, non-toxic, near-infrared-emitting Au cluster-protein nanoconjugates for targeted cancer imaging *Nanotechnol.* **21** 055103
- [7] Lin C A *et al* 2009 Synthesis, characterization, and bioconjugation of fluorescent gold nanoclusters toward biological labelling applications *ACS Nano* **3** 395–401
- [8] Zhou R, Shi M, Chen X, Wang M and Chen H 2009 Atomically monodispersed and fluorescent sub-nanometer gold clusters created by biomolecule-assisted etching of nanometer-sized gold particles and rods *Chemistry* **15** 4944–51
- [9] Duan H and Nie S 2007 Etching colloidal gold nanocrystals with hyper-branched and multivalent polymers: a new route to fluorescent and water-soluble atomic clusters *J. Am. Chem. Soc.* **129** 2412–3
- [10] Templeton A, Chen S, Gross S and Murray M 1999 Water soluble, isolable gold clusters protected by tiopronin and coenzyme a monolayers *Langmuir* **15** 66–76
- [11] Lee D, Donkers R L, Wang G, Harper A S and Murray R W 2004 Electrochemistry and optical absorbance and luminescence of molecule-like Au₃₈ nanoparticles *J. Am. Chem. Soc.* **126** 6193–9
- [12] Paau M C, Lo C K, Yang X and Choi M M F 2010 Synthesis of 1.4 nm α -cyclodextrin-protected gold nanoparticles for luminescence sensing of mercury(II) with picomolar detection limit *J. Phys. Chem.* **114** 15995–6003
- [13] Sahib E S and Pradeep T 2011 Quantum clusters in cavities: trapped Au₁₅ in cyclodextrins *Chem. Mater.* **23** 989–99
- [14] Zhang H, Huang X, Li L, Zhang G, Hussain I, Li Z and Tan B 2012 Photoreductive synthesis of water-soluble fluorescent metal nanoclusters *Chem. Commun.* **48** 567–9
- [15] Shiraishi Y, Arakawa D and Toshima N 2002 pH-dependent color change of colloidal dispersions of gold nanoclusters: effect of stabilizer *Eur. Phys. J. E* **8** 377–83
- [16] Shang L, Azadfar N, Stockmar F, Send W, Trouillet V, Bruns M, Gerthsen D and Nienhaus G U 2011 One-pot synthesis of near-infrared fluorescent gold clusters for cellular fluorescence lifetime imaging *Small* **7** 2614–20
- [17] Chaki N K, Singh P, Dharmadhikari C V and Vijayamohan K P 2004 Single-electron charging features of larger, dodecanethiol-protected gold nanoclusters: electrochemical and scanning tunnelling microscopy studies *Langmuir* **20** 10208–17
- [18] Shang L, Dörlich R M, Brandholt S, Schneider R, Trouillet V, Bruns M, Gerthsen D and Nienhaus G U 2011 Facile preparation of water-soluble fluorescent gold nanoclusters for cellular imaging applications *Nanoscale* **3** 2009–14
- [19] Yao H, Miki K, Nishida N, Sasaki A and Kimura K 2005 Large optical activity of gold nanocluster enantiomers induced by a pair of optically active penicillamines *J. Am. Chem. Soc.* **127** 15536–43
- [20] Yang X, Gan L, Han L, Li D, Wang J and Wang E 2013 Facile preparation of chiral penicillamine protected gold nanoclusters and their applications in cell imaging *Chem. Commun.* 2302–4
- [21] Michalak M, Robert Parker J M and Opas M 2002 Ca²⁺ signalling and calcium binding chaperones of the endoplasmic reticulum *Cell Calcium* **32** 269–78
- [22] Dedhar S *et al* 1994 Inhibition of nuclear hormone receptor activity by calreticulin *Nature* **367** 480–3
- [23] Desai D, Michalak M, Singh N K and Niles R M 1996 Inhibition of retinoic acid receptor function and retinoic acid-regulated gene expression in mouse melanoma cells by calreticulin, a potential pathway for cyclic AMP regulation of retinoic action *J. Biol. Chem.* **271** 15153–9
- [24] Zamanian M, Veerakumarasivam A, Abdullah S and Rosli R 2013 Calreticulin and cancer *Pathol. Oncol. Res.* **19** 149–54
- [25] Gold L *et al* 2006 Overview of the role for calreticulin in the enhancement of wound healing through multiple biological effects *J. Investigative Dermatol.* **11** 57–65
- [26] Sheng V, Cheng C, Dong M, Zhou J, Liu Q, Dong Q and Li F 2014 Over-expression of calreticulin contributes to the development and progression of pancreatic cancer *J. Cell. Physiol.* **229** 887–97
- [27] Chen C N *et al* 2009 Identification of calreticulin as a prognosis marker and angiogenic regulator in human gastric cancer *Ann. Surg. Oncol.* **16** 524–33
- [28] Bini L *et al* 2009 Protein expression profiles in human breast ductal carcinoma and histologically normal tissue *Electrophoresis* **18** 2832–41
- [29] Obeid M *et al* 2007 Leveraging the immune system during chemotherapy: moving calreticulin to the cell surface converts apoptotic death from 'silent' to immunogenic *Cancer Res.* **67** 7941–4
- [30] Clarke C and Smyth M J 2007 Calreticulin exposure increases cancer immunogenicity *Nat. Biotechnol.* **25** 192–3
- [31] Obeid M *et al* 2007 Ecto-calreticulin in immunogenic chemotherapy *Immunol. Rev.* **220** 22–34
- [32] Chao M P *et al* 2010 Calreticulin is the dominant pro-phagocytic signal on multiple human cancers and is counterbalanced by CD47 *Sci. Transl. Med.* **2** 63ra94
- [33] Liu X, Li C, Xu J, Lv J, Zhu M, Guo Y, Cui S, Liu H, Wang S and Li Y 2008 Surfactant-free synthesis and functionalization of highly fluorescent gold quantum dots *J. Phys. Chem. C* **112** 10778–83
- [34] Crosby G and Demos J 1971 Measurement of photoluminescence quantum yields, review *J. Phys. Chem.* **75** 991–1024
- [35] Giorgakis E, Ramesh B, Kamali-Dashtarzheneh A, Fusai G K, Imper C, Tsironis D and Loizidou M 2016 Demonstration of calreticulin expression in hamster pancreatic adenocarcinoma with the use of fluorescent gold quantum dots *Anticancer Res.* **36** 861–7
- [36] Baker M 2010 Nanotechnology imaging probes: smaller and more stable *Nano Meth* **7** 957–62

- [37] Qu X, Li Y, Li L, Wang Y, Liang J and Liang J 2015 Fluorescent gold nanoclusters: synthesis and recent biological application *J. Nanomater.* **2015** 784097
- [38] Jiang W, Mardiyani S, Fischer H and Chan W C W 2006 Design and characterisation of lysine cross-linked mercapto-acid biocompatible quantum dots *Chem. Mater.* **18** 872–8
- [39] Borowicz P, Hotta J, Sasaki K and Masuhara H 1998 Chemical and optical mechanism of microparticle formation of poly (N-vinylcarbazole) in N,N-dimethylformamide by photon pressure of a focused near-infrared laser beam *J. Phys. Chem. B* **102** 1896–901
- [40] Bao H B, Gong Y J, Li Z and Gao M Y 2004 Enhancement effect of illumination on the photoluminescence of water-soluble CdTe nanocrystals: toward highly fluorescent CdTe/CdS core-shell structure *Chem. Mater.* **16** 3853–9
- [41] Wang F, Deng Rm Wang J, Wang Qm Han Ym Zhu H, Chen X and Liu X 2009 Tuning up conversion through energy migration in core-shell nanoparticles *Nat. Mater.* **10** 968–73
- [42] Pan Z, Lu Y Y and Feng L 2012 sunlight-activated long-persistent luminescence in the near-infrared from Cr³⁺-doped zinc gallogermanates *Nat. Mater.* **11** 58–63
- [43] Sun H, Zhang H, Ju J, Zhang J, Qian G, Wang C, Yang B and Wang Z Y 2008 One-step synthesis of high-quality gradient CdHgTe nanocrystals: a prerequisite to prepare CdHgTe/polymer bulk composites with intense near-infrared photoluminescence *Chem. Mater.* **20** 6764–9
- [44] Goswami N, Giri A, John R, Xavier P L, Pradeep T and Pal S K 2012 Protein-directed synthesis of NIR-emitting, tunable HgS quantum dots and their applications in metal-ion sensing *Small* **8** 3175–84
- [45] Dat C, Yang C X and Yan X P 2015 Ratiometric fluorescent detection of phosphate in aqueous solution based on near infrared fluorescent silvernanoclusters/metal-organic shell composite *Anal. Chem.* **87** 11455–9
- [46] Le Guével X, Perez Perrino M, Fernández T D, Palomares F, Torres M J, Blanca M, Rojo J and Mayorga C 2015 Glycosylation of fluorescent gold nanoclusters promotes increased human dendritic cell targeting via multiple endocytic pathways *ACS Appl. Mater. Interfaces* **7** 20945–56
- [47] Kageyama S, Isono T, Matsuda S, Ushio Y, Satomura S, Terai A, Arai Y, Kawakita M, Okada Y and Yoshiki T 2009 Urinary calreticulin in the diagnosis of bladder urothelial carcinoma *Int. J. Urol.* **16** 481–6